

Indium as a high cooling power nuclear refrigerant for quantum nanoelectronics

Nikolai Yurttagül,^{1,*} Matthew Sarsby,^{1,*} and Attila Geresdi^{1,†}

¹*QuTech and Kavli Institute of Nanoscience, Delft University of Technology, 2600 GA Delft, The Netherlands*

The frontiers of quantum electronics have been linked to the discovery of new refrigeration methods since the discovery of superconductivity at a temperature around 4K, enabled by the liquefaction of helium. Presently, nanoelectronic devices typically reach electron temperatures around 10 mK to 100 mK by commercially available dilution refrigerators. This led to discoveries such as the quantum Hall effect and new technologies like superconducting and semiconductor quantum bits. However, cooling electrons via the encompassing lattice vibrations, or phonons, becomes inefficient at low temperatures. Further progress towards lower temperatures requires new cooling methods for electrons on the nanoscale, such as direct cooling with nuclear spins, which themselves can be brought to microkelvin temperatures by adiabatic demagnetization. Here, we introduce indium as a nuclear refrigerant for nanoelectronics and demonstrate that solely on-chip cooling of electrons is possible down to a record low temperature of 3.2 ± 0.1 mK in an unmodified dilution refrigerator.

Quantum electronics relies on the precise control of electronic states in nanostructures, which is possible if the energy level separation is much higher than the thermal energy $k_B T$. Thus, the efficient cooling of electrons is vital for solid state nanoelectronics and is an important design consideration for existing scalable quantum technologies. Access to novel states of matter such as electron-nuclear ferromagnets [1–3], non-Abelian anyons in fractional quantum Hall states [4, 5], topological insulators [6] or exotic superconductivity [7–9] requires further progress in the cooling of nanoelectronics, approaching the μ K regime.

Typical electron temperatures of the order of 10 mK are accessible in semiconductor and metallic nanostructures by mounting the chip containing the devices on an insulating substrate cooled by commercially available dilution refrigerators. The lowest achievable electron temperature is limited by the heat transferred from the electrons at a temperature of T_e to phonons at a temperature of T_p . The heat flow between conduction electrons and phonons in a metallic volume V is $\dot{Q}_{ep} = \Sigma V (T_e^5 - T_p^5)$, where Σ is a material dependent coupling constant of the

order of $10^9 \text{ WK}^{-5} \text{ m}^{-3}$ [10, 11]. A residual heat leak of $\dot{Q}_{\text{leak}} = 10 \text{ aW}$ to a well-shielded nanostructure [12] with $V = 1 \mu\text{m}^3$ then yields $T_e \approx 25 \text{ mK}$ even as T_p approaches zero. Increasing the coupling volume V by electrodeposition of thick metal films and improving thermalization by liquid helium immersion cells led to $T_e \approx 4 \text{ mK}$ [13–15] in specially built dilution refrigerators.

The key to reduce the electron temperature further thus involves coupling the electron system to a cold bath without the necessity of heat transport via phonons. This can be achieved by nuclear magnetic cooling. In the limit of small Zeeman splitting compared to $k_B T_n$, the magnetization of the nuclear spin system is $M \propto B/T_n$ at a magnetic field of B and a temperature of T_n . T_n can be reduced by adiabatically lowering the magnetic field from B_i to B_f . In the absence of an external heat load, M stays constant and consequently $T_{n,f} = T_{n,i} \times B_f/B_i$ [16–18]. This technique has become the workhorse of ultralow-temperature physics, with the lowest attainable temperature of $T_n \sim 100 \text{ pK}$ [19].

On-chip nuclear magnetic cooling utilizes the spin-lattice relaxation to cool conduction electrons close to the temperature of a cold nuclear spin system which is co-integrated with the electronic device. The heat flow \dot{Q}_{en} is determined by the spin-lattice relaxation time τ_1 [20, 21]:

$$\dot{Q}_{\text{en}} = \tau_1^{-1} n C_n (T_n - T_n^2/T_e), \quad (1)$$

where C_n is the nuclear heat capacity and n is the molar amount of the nuclei. If the magnetization is weak, the Korringa-law $\tau_1 T_e = \kappa$ applies with the Korringa constant κ , and C_n can be approximated by the Schottky law $C_n = \alpha B^2/T_n^2$. Here, $\alpha = N_0 I(I+1) \mu_n^2 g_n^2 / 3k_B$ with I being the size of the nuclear spin, g_n the g-factor, N_0 , the Avogadro number and μ_n the nuclear magneton. In this limit, Eq. (1) reads

$$\dot{Q}_{\text{en}} = \alpha n \kappa^{-1} B^2 (T_e/T_n - 1). \quad (2)$$

The choice of nuclear refrigerant for nanoelectronics is based on finding a material with a large C_n , while keeping κ small to have efficient coupling to the electrons. Eq. (2) shows that the material-dependent figure of merit α/κ allows to compare different materials. In addition, the experimental implementation should allow for a large n and $B_i^2/T_{n,i}^2$ ratio for efficient cooling and long cold time.

Thus far, copper (Cu) was the sole material utilized for the nuclear cooling of nanoelectronics [22–24]. Naturally occurring Cu nuclei have a spin of $3/2$ yielding

* These authors contributed equally to this work.

† Corresponding author; e-mail: a.geresdi@tudelft.nl

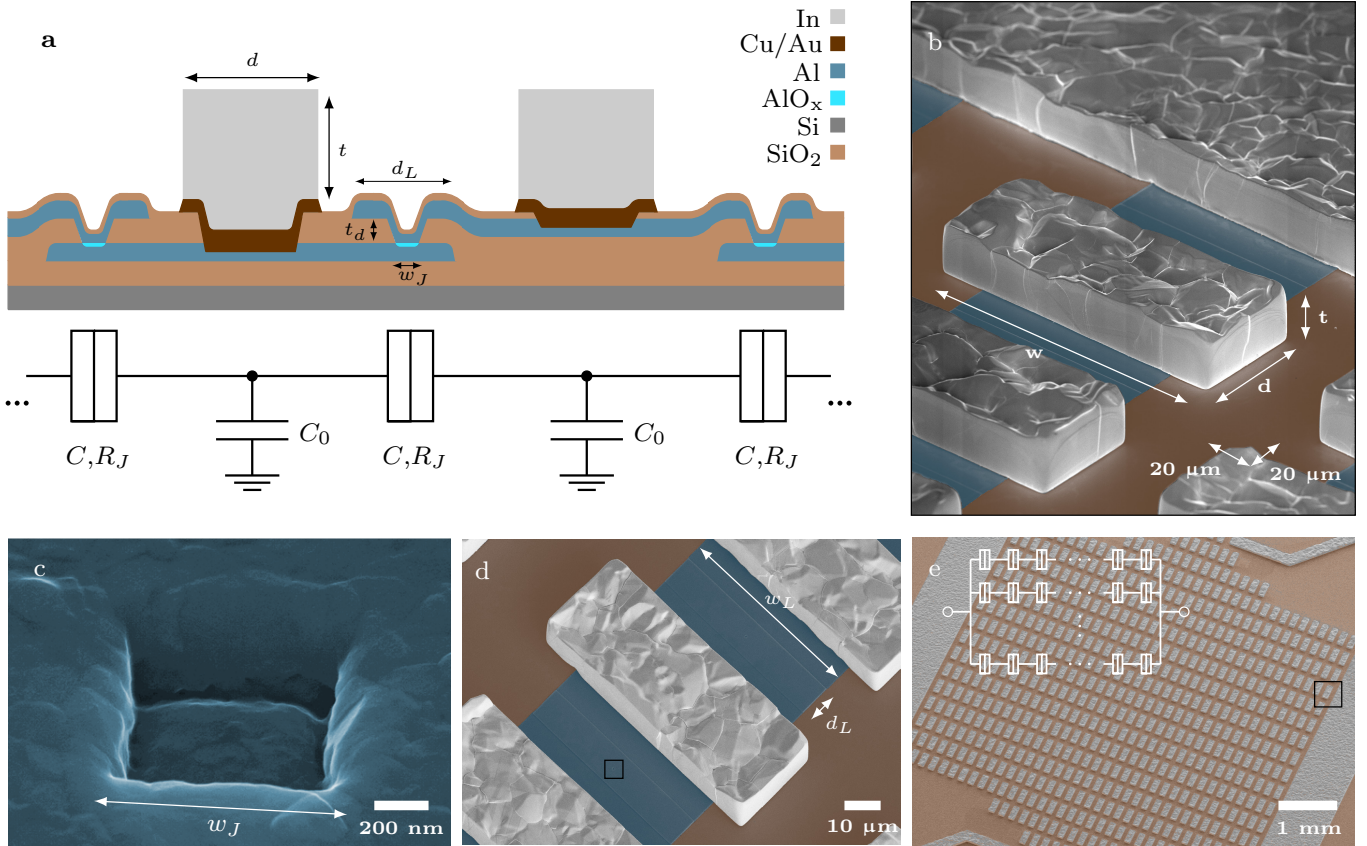


FIG. 1. **Integrated nuclear cooling and thermometry on chip.** (a) The cross-section and schematics of two metallic islands connected by Al-AIO_x-Al tunnel junctions with an area of w_J^2 and a resistance of R_J . The capacitance C is set by the overlap area $d_L \times w_L$ between the islands, whereas C_0 is the stray capacitance of each island. The electrons are cooled by the large volume In blocks electrodeposited onto the island. (b) False coloured scanning electron micrograph of a single In fin near the edge of the array. (c) Micrograph of a single AlO_x tunnel junction connecting adjacent islands in a row (d). The black square in panel (d) depicts the area shown in panel (c). (e) Overview of the full array with 35×15 islands. The black square depicts the area shown in panel (b).

$\alpha_{\text{Cu}} = 3.22 \mu\text{JKT}^{-2}\text{mol}^{-1}$ [21]. Bulk Cu nuclear demagnetization stages benefit from the low magnetic ordering temperature $< 0.1 \mu\text{K}$ [25], which allows for T_n values in the μK regime [26]. However, the weak electron-nucleus coupling given by $\kappa = 1.2 \text{ Ks}$ [20] is a limitation for electron cooling.

To overcome this limit, we utilize indium (In) as an on-chip nuclear refrigerant. In features a much shorter spin-lattice relaxation time characterized by $\kappa_{\text{In}} = 0.086 \text{ Ks}$ [27], and a large nuclear spin of $9/2$ with $\alpha_{\text{In}} = 13.8 \mu\text{JKT}^{-2}\text{mol}^{-1}$ enhancing the molar nuclear cooling power by a factor of $\frac{\alpha_{\text{In}}}{\kappa_{\text{In}}} / \frac{\alpha_{\text{Cu}}}{\kappa_{\text{Cu}}} = 60$ compared to Cu. We note that the lowest attainable T_n for In is limited by the tetragonal crystal field splitting of $250 \mu\text{K}$ [28]. In addition, the external magnetic field has to be kept above $B_c = 28 \text{ mT}$ to avoid the thermal decoupling of electrons by the superconducting phase transition [29].

COULOMB BLOCKADE THERMOMETRY WITH INTEGRATED INDIUM NUCLEAR REFRIGERANT

To demonstrate the applicability of In as a refrigerant for scalable nanoelectronics, we directly measure T_e in a nanoelectronic device while ramping B to perform the nuclear demagnetization. While primary electron thermometry in the millikelvin regime has been realized in several ways [10, 30–32], we utilize Coulomb blockade thermometry due to its lack of sensitivity to magnetic field [33]. These thermometers rely on the universal temperature dependence of single charge localization in mesoscopic metallic islands [34] and have been proposed to provide the reference scale for millikelvin range thermometry [35].

We integrate a nanofabricated Coulomb blockade thermometer (CBT) with In cooling blocks to directly cool the electrons inside the device (Fig. 1). The geometrical and electrical parameters of our thermometer are shown

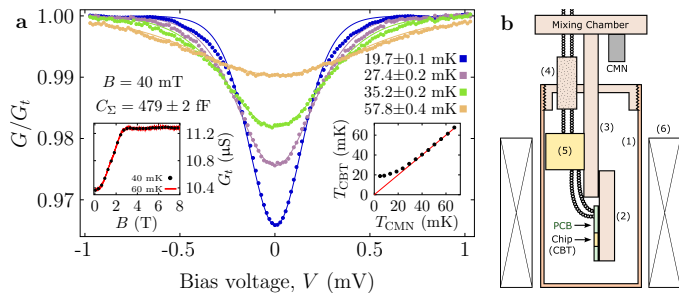


FIG. 2. Calibration of the Coulomb blockade thermometer and the cryogenic setup. **a** Normalized differential conductance G/G_t as a function of the voltage bias V at different temperatures with the solid lines showing the best fit determining the measured electron temperature T_{CBT} and the island capacitance $C_{\Sigma} = 479 \pm 2$ fF, see text. Right inset shows T_{CBT} as a function of the dilution refrigerator temperature T_{CMN} showing good thermalization for $T_{\text{CMN}} \gtrsim 30$ mK and a saturated $T_{\text{CBT}} \approx 20$ mK. These measurements were taken with an applied magnetic field $B = 40$ mT. The left inset shows the change of the high bias conductance G_t with magnetic field at two different temperatures. **b** Sketch of the cryogenic setup used in the experiment. The CBT chip is mounted to a Cu plate (2), attached to a mixing chamber of the dilution refrigerator by a Cu coldfinger (3). The sample is well shielded from electromagnetic noise by an RF-tight enclosure (1), Cu powder filters (4) and resistive low pass filters (5). The magnetic field is applied by a superconducting solenoid (6).

in Fig. 1a. The islands are formed within the stripe of $N = 36$ tunnel junctions, and each has a total capacitance $C_{\Sigma} = 2C + C_0$, which determines its effective charging energy $E_C = e^2/C_{\Sigma} \times (N - 1)/N$ with the elementary charge e . The zero bias conductance of the device, $G(V = 0)$ decreases by $\Delta G = G_t - G(V = 0) \sim E_C/k_B T_e$ in the limit of $E_C \ll k_B T_e$ [34] and retains its universal behavior down to $k_B T_e \approx 0.4 E_C$ with higher order corrections [36]:

$$\frac{\Delta G}{G_t} = u_N/6 - u_N^2/60 + u_N^3/630 - \dots, \quad (3)$$

with $u_N = E_C/k_B T_e$. Notably, the width of the conductance dip only depends on N , and $k_B T_e$, $eV_{1/2}/k_B T = 5.44N$ enabling primary thermometry without advance calibration [37]. We set E_C by the overlap area between adjacent islands, which is independent of the tunnel junction area determining R_J .

This flexibility in design is enabled by creating the Al-AlO_x-Al tunnel junctions *ex-situ* in vias through the interlayer dielectric (Fig. 1c) [38]. The junction area is $w_j^2 = 0.55 \pm 0.1 \mu\text{m}^2$ with a tunnel resistivity of $12.8 \pm 0.8 \text{ k}\Omega\mu\text{m}^2$ at room temperature, close to previously reported values [38], yielding a total device resistance $1/G_t = 55.8 \text{ k}\Omega$ in an array of $N \times M = 36 \times 15$ junctions. We note that the device resistance is temperature-dependent and saturates at $89 \text{ k}\Omega$ below

$T = 1 \text{ K}$ owing to the finite barrier height of the AlO_x insulating layer [39].

The CBT device used in this work was designed with an island overlap area of $w_L \times d_L = 18 \times 100 \mu\text{m}^2$ and an SiO₂ interlayer dielectric with a thickness of $t_d = 230 \text{ nm}$ (Fig. 1d). A parallel plate capacitor model $C = \epsilon_0 \epsilon_r A/d$ using $\epsilon_r = 3.5 - 3.9$ for sputtered SiO₂ [40] gives an estimated capacitance in the range of $C_{\Sigma} = 485 - 540 \text{ fF}$ corresponding to the CBT working as a primary thermometer between approximately 1.5 and 250 mK. This range is limited by uneven charge distribution on the low side [36] and instrumental resolution on the high side.

The nuclear magnetic cooling functionality is integrated by electroplating an In block with a volume of $50 \mu\text{m} \times 140 \mu\text{m} \times 25.4(1) \mu\text{m}$ through a thick photoresist mask onto each island (Fig. 1b). We achieve an In integration density of $1.6 \text{ pmol}/\mu\text{m}^2$. This figure determines the nuclear cooling power \dot{Q}_{en} , see Eq. (2), per unit area. We note that electroplating with a constant current results in extensive crystallization and hydrogen formation which decreases the density of the films and affects the patterning resolution. Therefore we apply forward and reverse current pulses to the electrochemical cell to refine the grain structure and reach a patterning resolution of $1 \mu\text{m}$ (see Supplementary Information for sample fabrication details).

The device is mounted onto a Cu carrier block inside an RF-tight enclosure cooled by an unmodified commercial wet dilution refrigerator [41]. The mixing chamber temperature is measured by a calibrated cerium magnesium nitrate (CMN) thermometer, and the base temperature is found to be approximately 5 mK. The scheme of the measurement setup is shown in Fig. 2b. The CBT is attached in a four wire geometry with the twisted pairs of the electrical wiring passing through a Cu powder [42] and a discrete component 3rd order RC low-pass filter, which has a cutoff frequency of 50 kHz to reduce external noise. The differential conductance $G(V)$ of the CBT is measured using standard low frequency (18.31 Hz) lockin techniques as a function of the DC voltage bias, V .

First we determine E_C by simultaneously fitting a set of $G(V)$ curves against the full single electron tunneling model [34] at different T_{CMN} values set by heating the mixing chamber (Fig. 2a). We find a $C_{\Sigma} = 479 \pm 2 \text{ fF}$, close to the designed value yielding $E_C = 330 \text{ neV}$. The measured electron temperature T_{CBT} agrees well with T_{CMN} for temperatures above 30 mK, but decouples and saturates for lower values, demonstrating the inefficiency of phonon cooling via the device substrate (right inset of Fig. 2a). We note that our device exhibits a slightly B -dependent G_t (left inset of Fig. 2a). This magnetoresistance is however independent of the device temperature below 100 mK and therefore can be accounted for during the demagnetization cycles. The established calibration of the CBT enables its use in a secondary mode of operation, by measuring the zero bias conductance decrease

and finding T_{CBT} based on Eq. (3). This mode avoids additional Joule heating at finite bias voltages and allows for a real-time temperature sampling whilst ramping the magnetic field.

ON-CHIP NUCLEAR MAGNETIC COOLING

To perform the nuclear demagnetization experiment, we first set the initial field B_i and let the CBT thermalize while the heat released by nuclear spin magnetization is absorbed by the dilution refrigerator. We find a typical $T_{\text{CBT}} \approx 20$ mK after 24 hours and $T_{\text{CBT}} \approx 16$ mK after 72 hours of precooling at $B_i = 12.8$ T. Then we reduce the field to $B_f < B_i$ with a constant rate \dot{B} whilst measuring the zero bias conductance $G(V = 0)$ of the CBT. We continuously track the conductance minimum in a dynamic bias window of ≈ 20 μV to compensate for voltage bias drifts over the several hours timescale of the experiment.

A typical experimental run starting from $B_i = 12.8$ T is shown in Fig. 3a. We set a magnetic field ramp rate $\dot{B} = -0.4$ mT/s and a final field $B_f = 40$ mT. The strong electron-nucleus coupling results in a reduction of the electron temperature T_{CBT} from its initial value of 16 mK, while $T_{\text{CMN}} \approx 5$ mK remains essentially constant. During the demagnetization cycle, we measure the curvature of the Coulomb-blockade peak and find excellent agreement with the model calculations based on the already inferred E_C for each temperature datapoint with no additional fit parameters (Fig. 3b). This analysis confirms the primary nature of our CBT thermometer throughout the entire temperature range of the experiment.

Here we find a record low electron temperature of $T_e = 3.2 \pm 0.1$ mK after on-chip demagnetization, with previously reported values reaching $T_e = 4.7$ mK, utilizing Cu as nuclear refrigerant [24]. We also demonstrate superior performance compared to helium immersion cells, where values above $T_e = 3.9$ mK were measured in a custom dilution refrigerator [15]. We compare our data with prior work in the inset of Fig. 3a and note that our results are comparable to [23] where $T_e = 2.8$ mK was achieved by a combination of on- and off-chip Cu nuclear cooling stages.

Upon reaching the lowest temperature at $B \approx 2$ T, the stage warms up quickly, and after the field ramp stops at $B_f = 40$ mT, it relaxes to the starting temperature. This behaviour indicates that the nuclear heat capacity depletes by parasitic heat leaks before the field ramp is finished. We analyze the cooling performance and heat leaks of our device by performing demagnetization runs at different \dot{B} between -0.3 mT/s and -6 mT/s (Fig. 4a). All data exhibit a similar behaviour with a minimum temperature well below $T_{\text{CMN}} \approx 5$ mK. In order to determine the heat input by parasitic heating we numerically

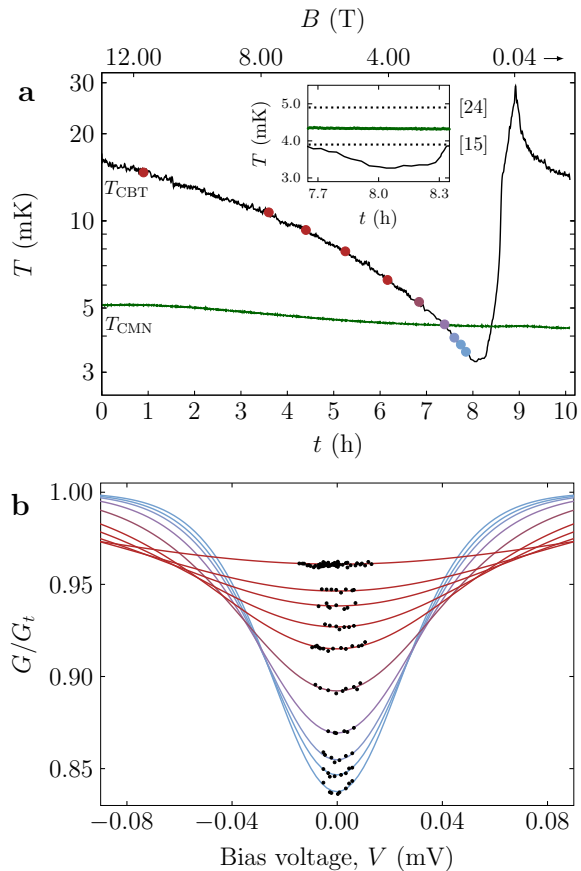


FIG. 3. **On-chip nuclear cooling experiment.** (a) The electron temperature T_{CBT} and the refrigerator temperature T_{CMN} while reducing the field from 12.8 T and 16 mK to 40 mT with $\dot{B} = -0.4$ mT/s including a 1 h thermal relaxation period at the end. Note that $T_{\text{CBT}} < T_{\text{CMN}}$ is clearly obtained. We show this part of the data in detail in the inset together with previously reported lowest electron temperatures for phonon cooling [15] and for on-chip nuclear cooling [24] experiments as dotted lines, respectively. (b) The normalized conductance at small voltage biases (black dots) at different temperatures confirms the expected zero bias curvature of the CBT calibration curve, see text. The position of each curve during the cooling run is shown by dots of the corresponding color in panel (a), respectively. Note the tenfold decrease in the bias voltage range compared to Fig. 2a.

model the time evolution of T_n and T_e on a single island. We neglect the weak thermal coupling to phonons and assume that the heat flow between the electrons and nuclei is described by Eq. (1). We consider the Hamiltonian of the nuclear spin where the interaction of the nuclear quadrupole moment with the crystal field gradient is included with $e^2 q Q = -198$ μeV [28]:

$$\mathbf{H} = -\gamma B \mathbf{I}_z + \frac{e^2 q Q}{4I(2I-1)} (3\mathbf{I}_z - \mathbf{I}^2). \quad (4)$$

The set of eigenvalues, ε_m , defines the partition sum $Z = \sum \exp(-\varepsilon_m/k_B T_n)$, which yields the nuclear spin

entropy $S_n = k_B \partial(T_n \log Z) / \partial T_n$ and the heat capacity $C_n = T_n (\partial S_n / \partial T_n)_B$. The time evolution of the temperatures is then as follows:

$$\begin{aligned} \frac{dT_n}{dt} &= \frac{T_e T_n - T_n^2}{\kappa} + \frac{\partial T_n}{\partial B} \dot{B}, \\ \frac{dT_e}{dt} &= -\frac{C_n}{C_e} \left(\frac{T_e T_n - T_n^2}{\kappa} \right) + \frac{\dot{Q}_{\text{leak}}}{nC_e}. \end{aligned} \quad (5)$$

The heat capacity of the electron system is assumed to follow the Sommerfeld rule, $C_e = \gamma T_e$, and we include a parasitic heat leak \dot{Q}_{leak} as a free parameter. Evaluating the experimental data in Fig. 4a, we plot $\dot{Q}_{\text{leak}}(B)$ in the upper inset of Fig. 4a and find the same behaviour independent of \dot{B} with a linear increase at high fields and a rapid upturn below 2 T. We evaluate the linear segment and find that the dissipation \dot{Q}_{leak} changes linearly with \dot{B} (lower inset of Fig. 4), $\dot{Q}_{\text{leak}} = a|\dot{B}| + \dot{Q}_0$ with $a = 18 \text{ pW}/(\text{mT s}^{-1})$ and $\dot{Q}_0 = 0.18 \text{ fW}$ per island. Notably, the largest measured heat leak per island is 108 fW corresponding to a total heat leak of 60 pW for the chip, exceeding earlier reported values in similar experiments [23, 24]. The linear $\dot{Q}_{\text{leak}}(\dot{B})$ is in striking contrast with observations on macroscopically large nuclear cooling stages, where eddy currents in the bulk refrigerant lead to a $\dot{Q}_{\text{leak}} \propto \dot{B}^2$ [21]. It is also inconsistent with a dominating static heat leak yielding a constant \dot{Q}_{leak} , or with an environmental coupling of $\dot{Q}_{\text{leak}} \propto T_e^n - T_{\text{env}}^n$. This confirms that the metallic islands of the CBT are thermally well decoupled from the environment, however the rate-independent \dot{Q}_{leak} suggests the presence of a local, on-island source of heat leak consuming the In nuclear heat capacity over the timescale of the experiment.

We evaluate the performance of electroplated In as an on-chip electron refrigerant by considering the nuclear heat capacity integrated on-chip per unit area, $\alpha' = \alpha n/A$ and use α'/κ as a figure of merit containing both the material parameters and the device geometry. Our device features $\alpha'/\kappa_{\text{In}} = 250 \text{ } \mu\text{W}/(\text{m}^2 \text{KT}^2)$, which is a factor of 3300 increase compared to $\alpha'/\kappa_{\text{Cu}} = 0.076 \text{ } \mu\text{W}/(\text{m}^2 \text{KT}^2)$ implemented in [23], clearly substantiating the merits of our approach.

We use Eq. (5) to model the behaviour of a Cu nuclear stage of the same volume exposed to the same \dot{Q}_{leak} in place of our In cooling blocks. The results are shown in Fig. 4b, together with our experimental data at $\dot{B} = -0.4 \text{ mT/s}$. Our simulations confirm that the In nuclei are strongly coupled to the electron system, resulting in $T_n = T_e$ throughout the entire experiment. In contrast, the weaker hyperfine coupling of Cu results in a deviation between T_n and T_e already at $T_e > 6 \text{ mK}$ demonstrating the limitations of Cu as an on-chip refrigerant. Furthermore, under the same experimental conditions, a Cu island of the same volume would have saturated at $T_e \approx 5.5 \text{ mK} > T_{\text{CMN}}$ due to its lower heat capacity.

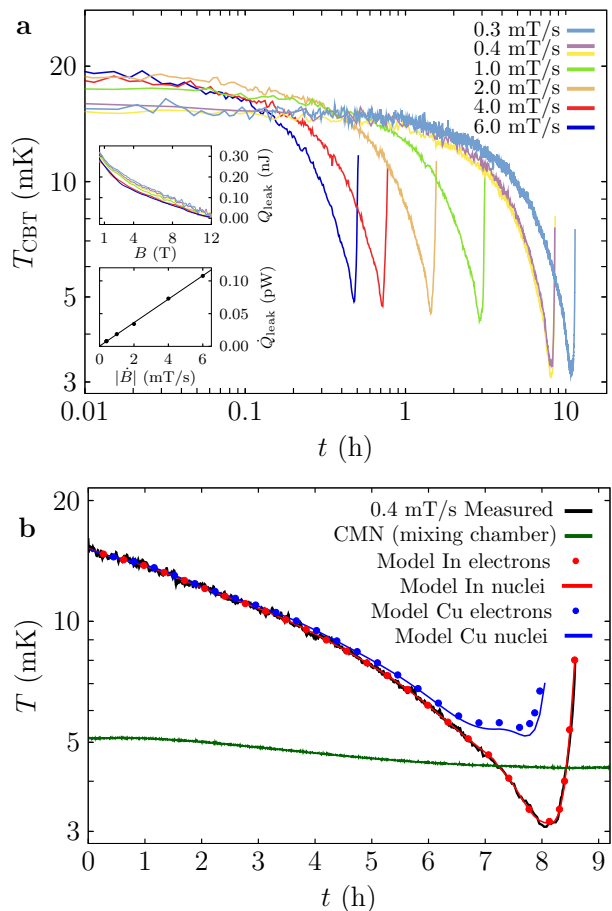


FIG. 4. **Electron cooling at different field ramp rates and device simulations.** (a) T_{CBT} as a function of time for various magnetic field ramp rates, \dot{B} . Two distinct runs with $\dot{B} = -0.4 \text{ mT/s}$ are shown to demonstrate the reproducibility of the data. The lower inset shows the extracted heat leak \dot{Q}_{leak} per island (black dots) and a linear fit (solid line). The upper inset demonstrates that the total absorbed heat \dot{Q}_{leak} per island collapses onto a single curve for all runs, see text. (b) Benchmarks of In and Cu as nuclear refrigerant simulated with the same experimental conditions, overlain with the measured T_{CBT} (black line) and T_{CMN} (green line) for $\dot{B} = -0.4 \text{ mT/s}$.

CONCLUSIONS

We demonstrated that electron temperatures of $3.2 \pm 0.1 \text{ mK}$ can be reached by nuclear magnetic cooling on-chip with In as nuclear refrigerant, a result that is the coldest measured electron temperature without additional off-chip nuclear demagnetization cooling. Using electrochemical film deposition methods, we integrate $1.6 \text{ pmol}/\mu\text{m}^2$ of In on our device. This, considering the material parameters as well, gives rise to more than three orders of magnitude increase in the on-chip integrated cooling power of electrons compared to state-of-the-art devices utilizing Cu thin films. Furthermore, In is the

preferred material of cryogenic interconnects [43], which provides the possibility to integrate In refrigerant in scalable quantum bit architectures. We also show that the on-chip cooling of nanoelectronics is viable despite a large molar heat leak of $0.8 \mu\text{W/mol}$. This value is to be compared to typical heat leaks of well isolated macroscopic demagnetization stages, generally falling in the range of 0.1 nW/mol to 1 nW/mol [18]. We therefore conclude that on-chip integrated nuclear refrigeration using In can provide a fast turnaround platform to decrease the electron temperature in existing cryogenic setups. Furthermore, the combination of on-chip and off-chip In refrigeration provides a promising route towards quantum nanoelectronics below 1 mK.

CORRESPONDING AUTHOR

Correspondence and request of materials should be addressed to Attila Geresdi.

ACKNOWLEDGEMENTS

The authors thank J. Mensingh and R. N. Schouten for technical assistance. We acknowledge O. Benningshof, J. Pekola and R. Haley for fruitful discussions and comments on the manuscript. This work has been supported by the Netherlands Organization for Scientific Research (NWO) and Microsoft Corporation Station Q.

AUTHOR CONTRIBUTIONS

M. S. and N. Y. performed the experiments and developed the framework to analyze the data. N. Y. designed and fabricated the devices. M. S. analyzed the data. A. G. designed and supervised the experiments. The manuscript has been prepared with contributions from all the authors.

DATA AVAILABILITY

Raw datasets measured and analysed for this publication are available at the 4TU.ResearchData repository, DOI: 10.4121/uuid:49b61cac-31c4-4922-b541-2e7270652e9b (Ref. [44]).

[1] Deshpande, V. V., Bockrath, M., Glazman, L. I. & Yacoby, A. Electron liquids and solids in one dimension. *Nature* **464**, 209 (2010).

- [2] Braunecker, B., Simon, P. & Loss, D. Nuclear magnetism and electron order in interacting one-dimensional conductors. *Physical Review B* **80**, 165119 (2009).
- [3] Chekhovich, E. *et al.* Nuclear spin effects in semiconductor quantum dots. *Nature materials* **12**, 494 (2013).
- [4] Nayak, C., Simon, S. H., Stern, A., Freedman, M. & Das Sarma, S. Non-Abelian anyons and topological quantum computation. *Rev. Mod. Phys.* **80**, 1083–1159 (2008).
- [5] Stern, A. Non-Abelian states of matter. *Nature* **464**, 187 (2010).
- [6] Hasan, M. Z. & Kane, C. L. Colloquium: Topological insulators. *Rev. Mod. Phys.* **82**, 3045–3067 (2010).
- [7] Mackenzie, A. P. & Maeno, Y. The superconductivity of Sr_2RuO_4 and the physics of spin-triplet pairing. *Rev. Mod. Phys.* **75**, 657–712 (2003).
- [8] Vojta, M. Quantum phase transitions. *Reports on Progress in Physics* **66**, 2069 (2003).
- [9] Klinovaja, J., Stano, P., Yazdani, A. & Loss, D. Topological superconductivity and Majorana fermions in RKKY systems. *Phys. Rev. Lett.* **111**, 186805 (2013).
- [10] Giazotto, F., Heikkilä, T. T., Luukanen, A., Savin, A. M. & Pekola, J. P. Opportunities for mesoscopics in thermometry and refrigeration: Physics and applications. *Rev. Mod. Phys.* **78**, 217–274 (2006).
- [11] Wellstood, F., Urbina, C. & Clarke, J. Hot-electron effects in metals. *Physical Review B* **49**, 5942 (1993).
- [12] Saira, O.-P., Kemppinen, A., Maisi, V. F. & Pekola, J. P. Vanishing quasiparticle density in a hybrid Al/Cu/Al single-electron transistor. *Phys. Rev. B* **85**, 012504 (2012).
- [13] Xia, J. *et al.* Ultra-low-temperature cooling of two-dimensional electron gas. *Physica B: Condensed Matter* **280**, 491 – 492 (2000).
- [14] Samkharadze, N. *et al.* Integrated electronic transport and thermometry at millikelvin temperatures and in strong magnetic fields. *Review of Scientific Instruments* **82**, 053902 (2011).
- [15] Bradley, D. I. *et al.* Nanoelectronic primary thermometry below 4 mK. *Nature communications* **7**, 10455 (2016).
- [16] Gorter, C. J. Kernentmagnetisierung. *Phys. Z.* **35**, 923 (1934).
- [17] Kurti, N., Robinson, F. H., Simon, F. & Spohr, D. Nuclear cooling. *Nature* **178**, 450 (1956).
- [18] Andres, K. & Lounasmaa, O. Recent progress in nuclear cooling. In *Progress in Low Temperature Physics*, vol. 8, 221–287 (Elsevier, 1982).
- [19] Knuuttila, T. A., Tuoriniemi, J. T. & Lefmann, K. Relaxation of polarized nuclei in superconducting rhodium. *Phys. Rev. Lett.* **85**, 2573–2576 (2000).
- [20] Enss, C. & Hunklinger, S. *Low-Temperature Physics*, vol. 1 (Springer, 2005).
- [21] Pobell, F. *Matter and methods at low temperatures*, vol. 2 (Springer, 2007).
- [22] Clark, A. C., Schwarzwälder, K. K., Bandi, T., Maradan, D. & Zumbühl, D. M. Method for cooling nanostructures to microkelvin temperatures. *Review of Scientific Instruments* **81**, 103904 (2010).
- [23] Palma, M. *et al.* On-and-off chip cooling of a Coulomb blockade thermometer down to 2.8 mK. *Applied Physics Letters* **111**, 253105 (2017).
- [24] Bradley, D. *et al.* On-chip magnetic cooling of a nanoelectronic device. *Scientific Reports* **7**, 45566 (2017).

- [25] Symko, O. Nuclear cooling using copper and indium. *Journal of Low Temperature Physics* **1**, 451–467 (1969).
- [26] Xu, J. *et al.* Nuclear demagnetization cryostat at University of Florida Microkelvin Laboratory. *Journal of Low Temperature Physics* **89**, 719–722 (1992).
- [27] MacLaughlin, D. & Butterworth, J. Nuclear spin-lattice relaxation in indium metal by NQR. *Physics Letters* **23**, 291 (1966).
- [28] Tang, Y., Adams, E., Uhlig, K. & Bittner, D. Nuclear cooling and the quadrupole interaction of indium. *Journal of Low Temperature Physics* **60**, 352–363 (1985).
- [29] Tinkham, M. *Introduction to superconductivity* (Courier Corporation, 1996).
- [30] Spietz, L., Lehnert, K. W., Siddiqi, I. & Schoelkopf, R. J. Primary electronic thermometry using the shot noise of a tunnel junction. *Science* **300**, 1929–1932 (2003).
- [31] Feshchenko, A. *et al.* Tunnel-junction thermometry down to millikelvin temperatures. *Physical Review Applied* **4**, 034001 (2015).
- [32] Iftikhar, Z. *et al.* Primary thermometry triad at 6mK in mesoscopic circuits. *Nature Communications* **7**, 12908 (2016).
- [33] Pekola, J. P. *et al.* Coulomb blockade-based nanothermometry in strong magnetic fields. *Journal of Applied Physics* **83**, 5582–5584 (1998).
- [34] Pekola, J. P., Hirvi, K. P., Kauppinen, J. P. & Paalanen, M. A. Thermometry by arrays of tunnel junctions. *Phys. Rev. Lett.* **73**, 2903–2906 (1994).
- [35] Meschke, M., Engert, J., Heyer, D. & Pekola, J. P. Comparison of Coulomb blockade thermometers with the international temperature scale PLTS-2000. *International Journal of Thermophysics* **32**, 1378 (2011).
- [36] Feshchenko, A. *et al.* Primary thermometry in the intermediate Coulomb blockade regime. *Journal of Low Temperature Physics* **173**, 36–44 (2013).
- [37] Farhangfar, S., Hirvi, K., Kauppinen, J., Pekola, J. & Toppari, J. One dimensional arrays and solitary tunnel junctions in the weak Coulomb blockade regime: CBT thermometry. *Journal of Low Temperature Physics* **108**, 191–215 (1997).
- [38] Prunnila, M. *et al.* Ex situ tunnel junction process technique characterized by Coulomb blockade thermometry. *Journal of Vacuum Science and Technology B* **28**, 1026 (2010).
- [39] Gloos, K., Poikolainen, R. S. & Pekola, J. P. Wide-range thermometer based on the temperature-dependent conductance of planar tunnel junctions. *Applied Physics Letters* **77**, 2915–2917 (2000).
- [40] Reynard, J. *et al.* Integration of fluorine-doped silicon oxide in copper pilot line for 0.12 μm technology. *Microelectronic Engineering* **60**, 113–118 (2002).
- [41] MNK126-700. Leiden Cryogenics.
- [42] Mueller, F. *et al.* Printed circuit board metal powder filters for low electron temperatures. *Review of Scientific Instruments* **84**, 044706 (2013).
- [43] Rosenberg, D. *et al.* 3D integrated superconducting qubits. *npj Quantum Information* **3**, 42– (2017).
- [44] Yurttagul, N., Sarsby, M. & Geresdi, A. Indium as a high cooling power nuclear refrigerant for quantum nanoelectronics. 4TU.ResearchData repository. <http://dx.doi.org/10.4121/uuid:49b61cac-31c4-4922-b541-2e7270652e9b>.